Received: 7 January 2019 | Revised: 17 March 2019 | Accepted: 18 March 2019

DOI: 10.1002/er.4563

RESEARCH ARTICLE

WILEY INTERNATIONAL JOURNAL OF ENERGY RESEARCH

Planar and textured surface optimization for a tritium-based betavoltaic nuclear battery

Johnny Russo[1,4] | Marc S. Litz[1] | I.I. William Ray[2] | Hakan Berk[3] | Hansol Cho[4] | David I. Bigio[4] | Adam Weltz[6] | Tariq Rizvi Alam[5,6]

[1]Sensors and Electron Devices Directorate, US Army Research Laboratory, Adelphi, Maryland

[2]Department of Electrical Engineering, Texas Tech University, Lubbock, Texas

[3]Department of Electrical Engineering, University of Maryland, College Park, Maryland

[4]Department of Mechanical Engineering, University of Maryland, College Park, Maryland

[5]National Strategic Research Institute (NSRI), University of Nebraska, Omaha, Nebraska

[6]Nuclear Technologies Survivability (NTS), Defense Threat Reduction Agency (DTRA), Fort Belvoir, Virginia

Correspondence
Johnny Russo, Department of Mechanical Engineering, University of Maryland, College Park, Maryland 20742.
Email: john.a.russo20.civ@mail.mil

Summary

Remote, terrestrial, and space sensors require sources that have high enough power and energy densities for continuous operation for multiple decades. Conventional chemical sources have lower energy densities and lifetimes of 10 to 15 years depending on environmental conditions. Betavoltaic (βV) nuclear batteries using β^--emitting radioisotopes possess energy densities approximately 1000 times greater than conventional chemical sources. Their electrical power density ($P_{e,vol}$ in W/cm^3) in a given volume is a function of β^--flux surface power density $\left(P_{\beta^-}\right)$, surface interface type between radioisotope and transducer, β^- range, and transducer thickness and conversion efficiency (η_s). Tritium is the most viable β^--emitting radioisotope because of its commercial availability, low biotoxicity, half-life, and low energy, which minimizes the penetration depth and damage of transducer. To maximize $P_{e,vol}$, tritium in solid or liquid form must be used in the βV nuclear battery. A Monte Carlo source model using MCNP6 was developed to maximize the $P_{e,vol}$ of a tritium-based βV nuclear battery. First, a planar coupling configuration with different tritiated compounds (ie, titanium tritide and tritiated nitroxide) and a semiconductor transducer (4H-SiC) with thicknesses of 1 and 100 μm were modeled. The results showed that β^--source efficiency (η_β), which is the percentage of energy deposited in the transducer, decreased as the tritiated compound's mass density increased. The highest $P_{e,vol}$ was dependent on a combination of characteristics: specific activity (A_m in Ci/g), mass density, and 4H-SiC layer thickness. The tritiated nitroxide with the highest A_m at 2372 Ci/g produced the highest $P_{e,vol}$ at 2.46 mW/cm^3. Second, a 3-D coupling configuration was modelled to increase surface interfacing between the radioisotope source and textured transducer surface. 3-D coupling configuration increased the percentage of energy deposited into the transducer

List of Symbols, Abbreviations, and Acronyms: $2P_{\beta^-}$, bidirectional beta (β^-)-flux surface power density; 2-D, two-dimensional; 3-D, three-dimensional; A_m, specific activity; Be^3H_2, beryllium tritide; βV, betavoltaic; $D_{0.99}$, saturation layer thickness; D_L, radioisotope layer thickness; D_{opt}, optimal radioisotope layer thickness; E_{avg}, weighted arithmetic mean of beta (β^-) energy spectrum; E_{dep}, beta (β^-) energy deposited in matter; η_β or η_{tr}, beta (β^-) source efficiency; η_s or $\eta_{\beta\text{-}e}$, semiconductor conversion efficiency; η, total/system efficiency; MCNP6, Monte Carlo N-Particle Version 6; ^{63}Ni, nickel-63; nps, number of histories to run; ρ_m, mass density or bulk density; P_{β^-}, beta (β^-)-flux surface power density; $P_{e,vol}$, electrical power density; ^{147}Pm, promethium-147; RPS, radioisotope power source; SATP, standard ambient temperature and pressure; Sc^3H, scandium tritide; Ti^3H_x, titanium tritide/tritiated titanium hydride; ^{3}H, T, tritium; SiC or 4H-SiC, silicon carbide; S_m, effective surface activity or surface radioactivity; V_m, activity per unit volume; w, semiconductor converter feature width; a, radioisotope source width

because of more surface interfacing between the transducer and source in the same volume. The tritiated nitroxide was selected as the radioisotope source coupled with five different textured surface feature types. The $P_{e,vol}$ as a function of textured surface feature and gap, where the radioisotope is located, width was calculated for 1- and 100-μm 4H-SiC layer thicknesses. Results showed that η_β increased compared with planar coupling configuration (ie, approximately 56.2% increase over planar with cylindrical hole array) except with the rectangular pillar array. Still, the rectangular pillar array produced the highest $P_{e,vol}$ at 4.54 mW/cm^3 with an increasing factor of 2.29 compared with the planar coupling configuration.

KEYWORDS

Radioisotope Power Source, Tritium, MCNP, HARMST, Tritiated nitroxide, Textured surface, 4H-SiC, Nuclear Battery

1 | INTRODUCTION

Nuclear batteries, also called radioisotope power sources (RPSs), provide a continuous amount of power over a significantly longer lifetime than chemical-based power sources, especially when compared with a single charge/discharge cycle. Radioisotopes have energy densities several orders of magnitude higher than these chemical-based sources.[1] A nuclear battery's effectiveness is dependent on nine major factors shown in Table 1.[2] The research work described in this paper will be focused on five of the nine factors, which are circled and boldfaced in Table 1. The first factor is the type of ionizing radiation. Betavoltaic (βV) nuclear batteries are the most mature type of RPS with over 60 years of research, hundreds of prototypes, and a few commercially available products.[3] They are direct-conversion systems, converting β^- energy emission (type of ionizing radiation) into usable electrical energy through semiconductor energy conversion. Typically, the two components of the βV nuclear battery are the radioisotope source (carrier compound if needed) and semiconductor converter (βV cell), the transducer. Generally, the semiconductor converter is a solid-state PN or P-i-N diode. Presently, the βV nuclear batteries are the most efficient type of nuclear battery with the lowest volume.[3] Past and present prototypes are more energy dense with semiconductor efficiencies (η_s or $\eta_{\beta\text{-}e}$) ranging from 1% to 20% depending on the radioisotope and converter type.[3-5] Tritium ($^3H_2$ or T_2) is the most viable β^--emitting radioisotope for a terrestrial-based nuclear battery because of its commercial availability, low biotoxicity relative to other β^--emitters, lower energy β^--emitter (shallow penetration depth while minimizing all material damage), and half-life of 12.6 years.[6] The selection of tritium because of its attributes addresses the second factor.

The third and fourth factors relate directly to tritium's physical state as a gas in conditions and solutions of standard temperature and pressure and standard ambient temperature and pressure (SATP) with regard to its effective utilization in the nuclear battery. The standard approach to minimize nuclear-battery volume and contain tritium is metal tritides. The theoretical specific activity (A_m in Ci/g) range of the metal tritides is 605.39 Ci/g (Sc^3H) to 3860.8 Ci/g (Be^3H_2).[7] The most experimentally proven

TABLE 1 General nuclear-battery design factors to determine overall system potency[2]

Factor #	*Description*
1)	**Type of ionizing radiation**
2)	**Type of radioisotope**
3)	**Type of carrier compound where the radioisotope is embedded**
4)	**Ionizing radiation depth in carrier compound and any other surrounding matter**
5)	**Type of interface between ionizing radiation source and transducer**
6)	How transducer uses/loses and converts deposited energy from ionizing source
7)	Transducer conversion efficiency
8)	Type and magnitude/activity of carrier compound and transducer damage from ionizing radiation source
9)	How to extract energy from transducer

metal tritide is titanium tritide (Ti^3H_x), with a theoretical A_m of 1076 Ci/g to 1077.63 Ci/g based on Ti^3H_2. Based on published results, the highest and most stable titanium tritide was a foil that was approximately 81% to 83% loaded with tritium ($Ti^3H_{1.6}$ to $Ti^3H_{1.66}$) before $^3H_2$ outgassing and substantial surface flaking.[4] The major limitation with titanium tritide is the high mass density increases the self-absorption effect of the β^- particles, which is more evident with low β^- energies from 1 to 10 keV. The self-absorption effect influences the beta-source efficiency (η_β or η_{tr}), which is the β^- particle emission efficiency passing through the radioisotope and carrier layers and depositing into the semiconductor converter (transducer).[2] The experimental A_m and η_β limit the electrical power density ($P_{e,vol}$ in W/cm^3) and total or system efficiency (η) of the βV nuclear battery (Eqation 1) as follows:

$$\eta = \eta_\beta \eta_s. \quad (1)$$

The fifth factor is the type of interfacing or coupling between the radioisotope source and the semiconductor converter.[2] The goal of maximizing the transfer of beta energy emitted from the radioisotope into the transducer is addressed by this factor. The volume interface is where the radioisotope source is infused with the transducer, making it the optimal interface for all nuclear batteries. Increasing the effective surface area coupling between the radioisotope and transducer through the use of textured features (also called high aspect ratio or 3-D microstructures and/or nanostructures) on semiconductor surface increases surface power density. Extrapolating this increase in surface area coupling with a sponge-like structure where semiconductor microcavities are filled with radioisotope would lead to an increase in η_β and $P_{e,vol}$. The dimensions of semiconductor textured features and microcavity is dependent of radioisotope and semiconductor material type. This interface produces the highest percentage of ionizing-radiation energy deposition in the encapsulating transducer. However, this interface has never been demonstrated with a βV nuclear battery. The surface or planar interface, the most common interface type for βV nuclear batteries, couples the radioisotope source face or faces (top and bottom) with the transducer face or faces (top and bottom). The radioisotope is coated on the transducer surface. The surface interface's energy-deposition percentage is lower than the volume interface; the percentage difference is dependent on coupling configuration and radioisotope source type. The surface interface is limited by backscattering and semiconductor surface area. The radioisotope source means the pure radioisotope source and no other material (ie, carrier compound) when defining both interfaces. As a transitioning step toward the volume interface approach, a 3-D surface coupling configuration with a textured semiconductor surface and the radioisotope source are being developed and analyzed to achieve higher η_β and $P_{e,vol}$ compared with planar interface/coupling configuration.

Research efforts to increase the energy transfer between the radioisotope and transducer fall into three categories: 1) planar and 3-D coupling configuration optimization, 2) equal or similar transducer and radioisotope source volume, and 3) increase A_m and η_β. 1) the optimization of planar coupling configuration using analytical and numerical methods was attempted with metal tritides and SiC (transducer),[7] promethium-147 (^{147}Pm) and SiC (transducer),[8] and nickel-63 (^{63}Ni) and ^{147}Pm with various semiconductor converters.[5] Rahmani et al,[9] Kim et al,[1] and Wu et al[10] used a combination of closed form equations and Monte Carlo simulations to maximize nuclear and electrical power output based on a defined domain (i.e., radioisotope source layer thicknesses and dopant concentrations of the semiconductor junctions). However, η was never maximized nor prioritized in these publications.[7-11]

Optimization of 3-D coupling configuration with textured semiconductors and radioisotope source using experimental, analytical, and numerical methods was attempted with tritium gas and Si cylindrical array,[12] ^{63}Ni and GaN pyramidal and cylindrical pillar array,[13] and ^{147}Pm and hexagonal array.[14] These textures semiconductor surfaces are produced from high aspect ratio microstructure technology (HARMST).[15,16] In 2-3), based on Smart Cut process limits,[17,18] Alam et al designed a 1-cm^3 βV battery using multiple layers of planar sources and semiconductors and optimized the source thickness for the design.[7] After analyzing the research work, only two general conclusions are apparent because the research does not directly build off or relate to one another. First, periodic arrays, especially pillar arrays from growth processes, generate the highest $P_{e,vol}$, independent of radioisotope source.[13,14] Second, increasing A_m and η_β with mass density (ρ_m) between 0.5 and 1 g/cm^3 maximizes $P_{e,vol}$ with 1-μm-thick 4H-SiC layers.[7]

In this research we have worked on each described category and related our results to previous research, both experimental and numerical results. Starting with 3) we have identified two tritiated nitroxide compounds based on previous compounds[19,20] with higher A_m and lower mass densities than titanium tritides. In 1) these tritiated nitroxide compounds were compared with Ti^3H_x in planar coupling configuration using our numerical method. In 2) the tritiated compound with the highest $P_{e,vol}$ using 1- and 100-μm-thick 4H-SiC layers was implemented in 3-D coupling configuration using a similar numerical method. 3-D coupling configuration is a coupling

between all surfaces of the β^--emitting radioisotope source (fuel) and the textured semiconductor surface. Our numerical method results for the planar and 3-D configuration identifies the optimal tritiated compound and its thickness (D_L) and the textured feature array type and its dimensions, respectively. These optimal parameters (D_L, host material type, and textured surface feature type) maximize $P_{e,vol}$, thus shifting closer to the volume interface configuration's $P_{e,vol}$.

2 | APPROACH

A numerical method was developed to theoretically estimate the beta-flux power of several tritiated compounds. The beta-flux power was calculated by MCNP6 (Monte Carlo N-Particle Version 6) Transport Code. It is a general-purpose MC code that has the capability to model neutron, photon, and electron (or coupled) transport. The software can simulate transportation of particles with energy from 1 eV to 100 GeV based on evaluated data libraries. MCNP6 can generate a more realistic model compared with CASINO,[21] using more than one dimension, a full beta-energy spectrum rather than monoenergetic electron energies, the option to simulate isotropic, equiprobable beta-particle emission from within a source volume, and the ability to determine energy-deposition profiles in structures.[22] The beta spectrum of tritium was used in all simulations, both planar and 3-D configurations. With the Monte Carlo method, the results are obtained by simulating individual particles. The number of particle histories (nps) was 5×10^6 for all simulations that produced a relative error of less than 0.1. Simulation outputs were energy deposition (E_{dep} in MeV) and flux (cell particles/cm^2). This number of particles was simulated to obtain convergences for the results.

Two nuclear-battery configurations were modelled: planar (2-D) coupling configuration and 3-D coupling configuration. The shapes of the beta sources were cylindrical and rectangular volumetric sources depending on the configuration and textured surface feature type. 4H-SiC was used as the semiconductor converter in all simulations. 4H-SiC was chosen as the semiconductor converter because it has the highest semiconductor conversion efficiency (η_s) at 18.6% with tritium as the radioisotope source.[4]

2.1 | Numerical and experimental comparison with titanium tritide

The numerical method modelled titanium tritide (Ti^3H_x or TiT_x) with 4H-SiC to compare with previous experimental, empirical, and numerical data to confirm model validity. Therefore, the numerical method could then be used to model other tritiated compounds that are either in the beginning stages of development or presently theoretical. Ti^3H_x was chosen because it has an extensive amount of research and development in the past 50 years.[3,23,24] Kavetsky et al formulated the beta-flux surface power density ($P_{\beta^-}(D_L)$, $\left[\frac{W}{cm^2}\right]$) on the surface of a planar source and beta-source efficiency (η_β, [%]) of Ti^3H_2 equations based on empirical data.[25] The optimal layer thickness (D_{opt}) and saturation layer thickness ($D_{0.99}$) of the beta source are calculated from the two empirically based equations shown in Equations 2 and 3. Kavetsky et al considers the two thicknesses and beta-flux surface power density the most important parameters when determining and selecting the optimal tritiated compound for a nuclear battery.[25] Although the research work of Kavetsky et al uses a fully tritiated titanium tritide (Ti^3H_2), this metal tritide is only stable (presenting negligible tritium-gas leakage) when the foil or deposited layer is partially tritiated at a maximum range of 81% to 83% loaded. With deuterium ($^2H_2$), Ellis et al was able to load the titanium foils to 90% ($Ti^2H_{1.8}$), but after 52 days, it dropped to 75% ($Ti^2H_{1.5}$).[24] Thomas et al constructed a nuclear battery with a titanium tritide that was 81% to 83% loaded ($Ti^3H_{1.6}$ to $Ti^3H_{1.66}$) while remaining stable.[4] Based on previous work, Ti^3H_2 and $Ti^3H_{1.6}$ models were constructed using constant mass density of 3.91 g/cm^3 instead of a mass-density gradient from 3.92 g/cm^3 to 4.1 g/cm^3 for both titanium tritide foils.[19]

$$D_{opt} = D_L\left[\left(2P_{\beta^-} * \eta_\beta\right)_{max}\right], \tag{2}$$

$$D_{0.99} = D_{L_n}\left[100\% - \frac{2P_{\beta^-}{}_n - 2P_{\beta^-}{}_{n-1}}{2P_{\beta^-}{}_n} \approx 99\%\right], \tag{3}$$

where n is the counter or index number for the tritiated compound thickness input, D_L is the radioisotope layer thickness, $2P_{\beta^-}{}_n$ is the bidirectional β^--flux surface power density of D_{L_n} for which D_{L_n} equals $D_{0.99}$, and $2P_{\beta^-}{}_{n-1}$ is the bidirectional β^--flux surface power density of the previous tritiated compound thickness input, $D_{L_{n-1}}$.

2.2 | Numerical method of planar (2-D) coupling configuration

The planar coupling configuration, comprised of stacked disks, where the tritiated compound disk is fixed between

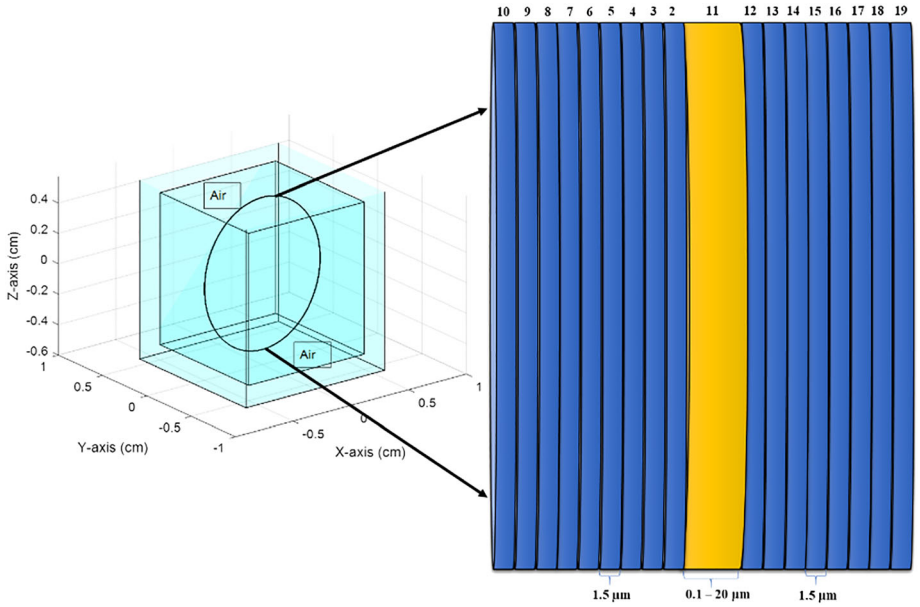

FIGURE 1 Illustrations of the planar coupling configuration in MCNP6. The tritiated compound layer (cell 11; orange) was placed between 4H-SiC layers (cell 2-10 and 12-19; blue) surrounded by air. The isotropic radioisotope source can be approximated as a bidirectional source because of the aspect ratio between the source thickness and diameter. Illustrations are not drawn to scale [Colour figure can be viewed at wileyonlinelibrary.com]

stacks of 4H-SiC disks, is shown in Figure 1. The 4H-SiC cell's or disk's thickness was 1.5 μm with a cell mass density (ρ_m) of 3.2 g/cm^3 and a total stack thickness of 9 μm on each side of the tritiated compound. The tritiated compound cell/disk's thickness (D_L) was varied from 100 nm to 20 μm, the defined domain. The radii of tritiated compound cells and 4H-SiC cells were 0.5 cm. Isotropic β^- particle emission was generated within each tritiated compound cell.

The beta-source efficiency (η_β, [%]) is the E_{dep} percentage deposited into the surrounding 4H-SiC cells. Curve fitting was formulated from E_{dep} percentage deposited into the 4H-SiC 1.5-μm cells on both sides of the tritiated compound. The total emitted activity or surface activity is calculated in Equation 4. The P_{β^-} is the product of the effective surface radioactivity (S_m), shown in Equation 4, and the weighted arithmetic mean of β^- energy spectrum (E_{avg}) through the tritiated nitroxide and into the 4H-SiC. As an approximation of the planar coupling configuration, we only account for the E_{dep} from the 4H-SiC disks on each side of the tritiated compound disk. This approximation is based on the aspect ratio of the tritiated compound thickness and diameter. The diameter is 50 times greater than the thickness. From this approximation, the beta emission is almost bidirectional even though it is simulated isotropically in MCNP6. The bidirectional β^- flux power ($2P_{\beta^-}$) is the β^- flux power emitted from both sides of the tritiated nitroxide disk for a 1-cm^2 footprint following the thin-film layer sources approach.[25]

$$S_m(D_L) = V(D_L) \times \rho_m \times \eta_\beta(D_L) \times A_m \times \frac{1}{A}; \left[\frac{Ci}{cm^2}\right], \quad (4)$$

where S_m, V, ρ_m, η_β, A_m, and A are the effective surface activity, volume, either bulk or true mass density, β^- source efficiency, specific activity, and area. The tritiated compounds simulated in the MCNP6 models are listed with relevant properties in Table 2.

In Table 2, M_W is molecular weight, ρ_m is either bulk or true mass density, GD is the weight percentage of ^{3}H, A_m is the specific activity, and V_m is the activity per unit volume of the tritiated compound. C3 and C4 are abbreviations for tritiated nitroxide Compounds 3 and 4, which are shown in Figure 2. Compound 3 is a five-membered nitroxide (3-(dipropargylamine)carboxamide-2,2,5,5-tetramethylpyrrolidinyloxyl); Compound 4 is a six-membered nitroxide (4-Oxo-2,2,6,6-tetra($^3H_3$)methyl-(3,3,5,5-$^3H_6$)piperidinyloxyl). C3 and C4 have already been hydrogenated and deuterated.[26] Tritiated nitroxide Compounds 1 and 2 (C1 and C2) were tritiated, stable, and demonstrated as radioisotope sources for a βV nuclear battery with using 4H-SiC βV cells.[19,20] The last set of numbers represents the bulk or true mass density of tritiated nitroxide C3 and C4. Different densities of the two tritiated nitroxides were simulated and analyzed because of variations in deposition procedure. Current procedure uses a micropipette to dispense the tritiated nitroxide, which is either a powder or oil depending on purity, in a solution with specific solvent on the converter

TABLE 2 Tritiated compound characteristics

Tritiated Compound Name	Chemical Composition	M_W (g/mol)	ρ_m (g/cm^3)	GD (^{3}H wt%)	A_m (Ci/g)	V_m (Ci/cm^3)
C30175	$C_{22}H_{26}{}^3H_{17}N_3O_3$	431	0.175[a]	12%	1150	201
C305	$C_{22}H_{26}{}^3H_{17}N_3O_3$	431	0.5[a]	12%	1150	576
C310175	$C_{22}H_{26}{}^3H_{17}N_3O_3$	431	1.0175[b]	12%	1150	1170
C401	$C_9{}^3H_{17}NO_2$	205	0.1[a]	25%	2372	237
C405	$C_9{}^3H_{17}NO_2$	205	0.5[a]	25%	2372	1186
C409	$C_9{}^3H_{17}NO_2$	205	0.9[b]	25%	2372	2135
Titanium Tritide	Ti^3H_2	54	3.91	12.5%	1076	4207

[a]Bulk density.

[b]Particle density or true mass density of a particulate solid or powder.

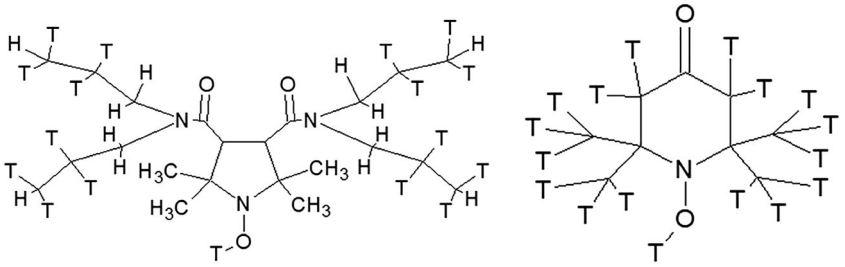

FIGURE 2 A, Chemical structures of five-membered tritiated nitroxide trioxylamine Compound 3; and B, six-membered tritiated nitroxide trioxylamine Compound 4. [$^3H_2 = T_2$]

surface (planar or textured). The density of the tritiated nitroxide coating is dependent on the concentration, solvent, converter surface, and use of reservoir adhered to the converter surface. These coating characteristics are being analyzed but not fully understood. So far, these coatings' densities are not equal to the particle or true mass density of the powder or oil, which is the main reason for the density-parameter study in MCNP6.

Two titanium tritides were simulated and analyzed in MCNP6. The fully tritiated titanium tritide chemical composition is Ti^3H_2; however, a stable version of this compound has never been created because of tritium desorption in a short timeframe.[27] For example, Ellis et al measured a deuterium loss of 19% (Ti^2H_2 to $Ti^2H_{1.6}$) after a week at SATP and additional deuterium loss of 6% ($Ti^2H_{1.6}$ to $Ti^2H_{1.5}$) after 4 days.[24] This experiment shows that deuterium loss is comparable with tritium loss. The maximum tritium concentration of powders and films is 65% ($Ti^3H_{1.3}$) and 85% ($Ti^3H_{1.7}$), respectively.[23] An 81% loaded titanium tritide ($Ti^3H_{1.6}$) was simulated to compare with the experimental results of Thomas et al.[4]

The 1-cm^3 nuclear-battery calculations were based on the planar-coupling, stacked configuration approach (Figure 3). The previous calculations identified the optimal parameters of 1-cm^2 footprint with tritiated compound layer thickness ranging from 100 nm to 20 μm, where optimal $2P_{\beta^-}$ is identified at $D_{0.99}$. This is considered the ideal battery configuration or packet: the tritiated compound

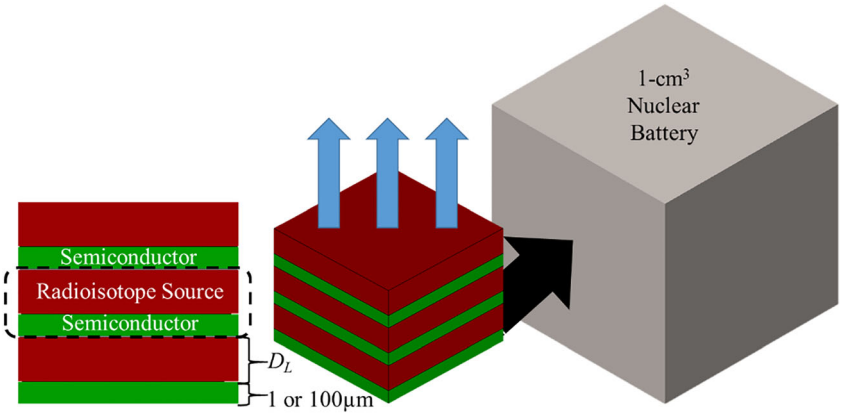

FIGURE 3 Illustrations of the planar-coupling, stacked configuration for a 1-cm^3 nuclear battery with either 1- or 100-μm-thick 4H-SiC layers. The semiconductor layer can convert from both sides in this concept, which is why there are not two semiconductors per radioisotope source. The 1-cm^2 radioisotope source and semiconductor transducer layers are stacked on top of each other to equal 1 cm in height. Illustrations are not drawn to scale [Colour figure can be viewed at wileyonlinelibrary.com]

(beta source) sandwiched between two semiconductors. It would be suitable for applications where area and total height is constrained to 1-cm^2 and a thickness less than 1 mm. The 1-cm^3 nuclear battery is made of the 1-cm^2 packets repeatedly stacked on top of each other to equal 1 cm in height. Two different semiconductor thicknesses were selected: 1 μm and 100 μm. The thicknesses represent the current (100 μm)[28,29] and future and ideal (1 μm)[17,18] thickness limits of the Smart Cut process using 4H-SiC material. For the 1-cm^2 nuclear battery packet, $2P_{\beta^-}$ was calculated as a function of D_L. For the 1-cm^3 nuclear battery, the electrical power density ($P_{e,vol}$, $[\frac{W}{cm^3}]$), activity per unit volume (V_m, $[\frac{Ci}{cm^3}]$), and number of packets as a function of source thickness (D_L) were calculated. The optimal D_L was identified at the maximum $P_{e,vol}$ for 1 μm and 100 μm thick 4H-SiC layers.

2.3 | Numerical method of 3-D coupling configuration

The planar coupling configuration approach is limited to two sides of the radioisotope source: top and bottom (Figure 3). In order to surpass the η_β and $P_{e,vol}$ limits with the planar interface approach, the coupling configuration between the radioisotope and transducer must transition from a planar to 3-D surface interface using a textured semiconductor surface. A numerical method was performed on five different 3-D coupling configurations with changing dimensions such as textured surface feature width ($\boldsymbol{w}$) and radioisotope source width ($\boldsymbol{a}$). Optimal textured surface features for each 3-D coupling configuration type were identified to maximize $P_{e,vol}$ while retaining a higher η_β than the planar coupling approach. The depth of the textured surface feature ($\boldsymbol{d}$) was constant at 10 μm for all simulations. The tritiated compound with the highest $P_{e,vol}$ from the planar coupling configuration was the radioisotope source used in the 3-D coupling configurations. The textured surface unit cell components comprise of the 4H-SiC textured feature and base, the 3-D coupling of the tritiated compound with the textured feature, and a top tritiated compound layer at the thickness where $P_{e,vol}$ (1-μm-thick 4H-SiC layers) of planar coupling configuration is maximum. Isotropic β^- particle emission was generated within each tritiated compound cell surrounding the feature and the layer on top. In the simulation and analysis, the ridge and rectangular arrays' beta-conversion volume included the base and textured surface feature. The ridge and rectangular arrays represent semiconductor-growth fabrication. The three other textured surface features represent semiconductor-etched fabrication.

Finally, the entire volume of the 4H-SiC converter can convert deposited beta energy at the same semiconductor-conversion efficiency (η_s). The assumption about constant η_s is based on the $\boldsymbol{w}$ parameter. Because of the radioisotope positioning, the energy being deposited into the semiconductor is all within the width of the textured semiconductor feature, $\boldsymbol{w}$. The collection region of beta energy in a semiconductor is defined as the depletion region, where charge collection is maximum and the diffusion current collection region. The semiconductors can be designed so the depletion region constitutes the majority of the energy deposition region based on the ratio of the charges in the P^+ and N region.[4] Thomas et al analyzed the diffusion current collection region in thin P^+N semiconductors and found the collection reaches 90% and above in semiconductors with thin P^+ regions and lightly doped N regions with surface recombination velocity below 10^5 cm/s. The depletion region width range is 1 to 4.6 μm[4,30]; its diffusion length (L_D) range is 1.5 to 12 μm.[2,4] Thus, because of the $\boldsymbol{w}$ parameter being set to a constant 1 μm, we assume the collection efficiency is the same for all shapes simulated, meaning a 100% chance of energy deposition in the depletion region because it is within the 1.5-μm depletion region width. Illustrations of all five different textured feature unit cells are shown in Figure 4. The unit-cell dimension limits are $100\ nm \leq \boldsymbol{a} \leq 10\ \mu m$, $\boldsymbol{w} = 1\ \mu m$, and $\boldsymbol{d} = 10\ \mu m$.

The $\boldsymbol{w}$ of the ridge, rectangular pillar, and rectangular-, hexagonal-, and cylindrical-hole arrays were set constant at 1 μm for all simulations based on previous planar MCNP6 simulations. Each tritiated compound listed in Table 2 was placed between two different semiconductors (4H-SiC and GaN, 4H-SiC and diamond, etc), as illustrated in Figure 5A. These wide bandgap semiconductors were selected because they will theoretically provide the highest semiconductor-conversion efficiency based on the Klein et al[31] and Olsen et al[32] curves. The normalized deposited beta energy as a function of semiconductor thickness was calculated and is depicted in Figure 5B. Approximately, 95% of the normalized energy was deposited within 1 μm of 4H-SiC, which is the semiconductor candidate for all simulations presented in this report. If the selected semiconductor were GaN or diamond, these feature dimensions would be thinner because the semiconductor-mass densities are higher, absorbing more beta energy with less converter volume.

Once the unit-cell dimension limits were set, the simulations were run matching the input file specifications stated in Section 2.2. The β^--flux surface power density (P_{β^-}) per textured feature unit cell was calculated as detailed in Section 2.2. The textured surface array P_{β^-} for a single layer was calculated by the product of the number of textured feature unit cells per 1 cm^2 and

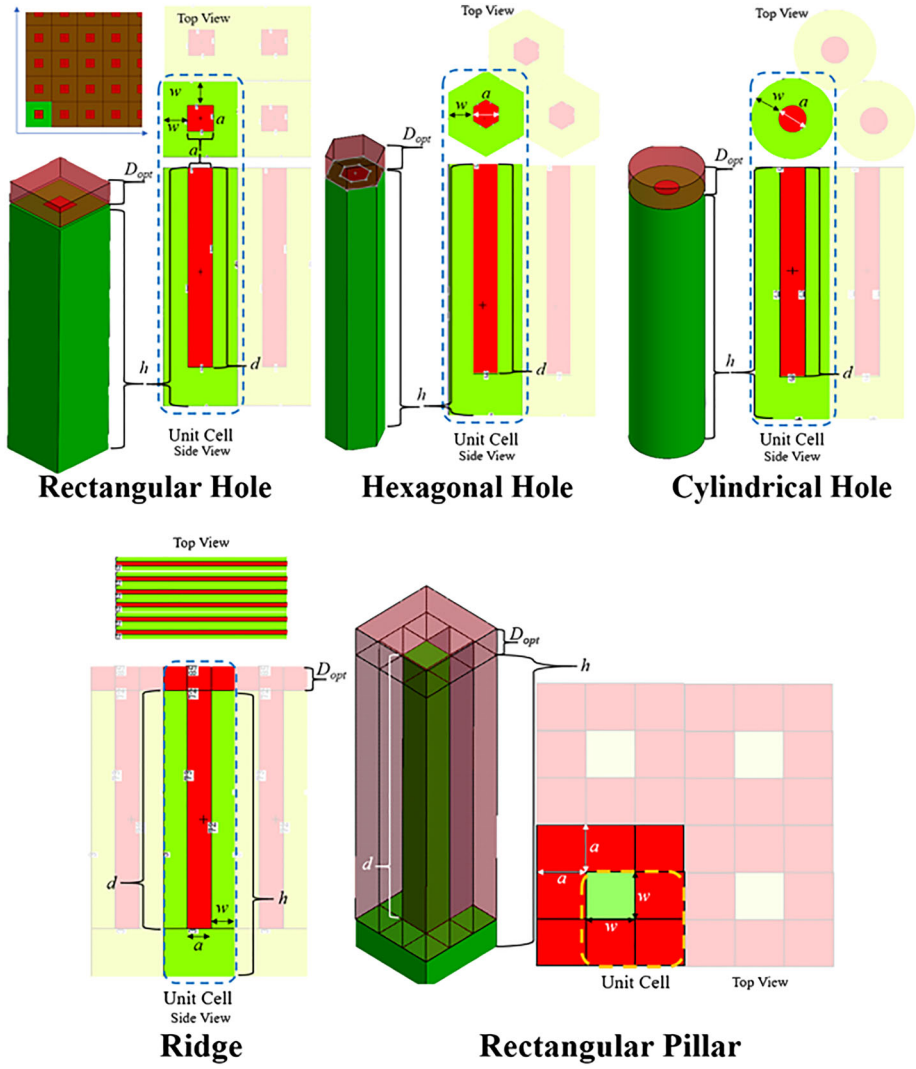

FIGURE 4 Illustrations of textured feature unit cells with labels for unit cell dimensions. The red cells are the radioisotope source cells and the green cells are the textured surface semiconductor transducer cells [Colour figure can be viewed at wileyonlinelibrary.com]

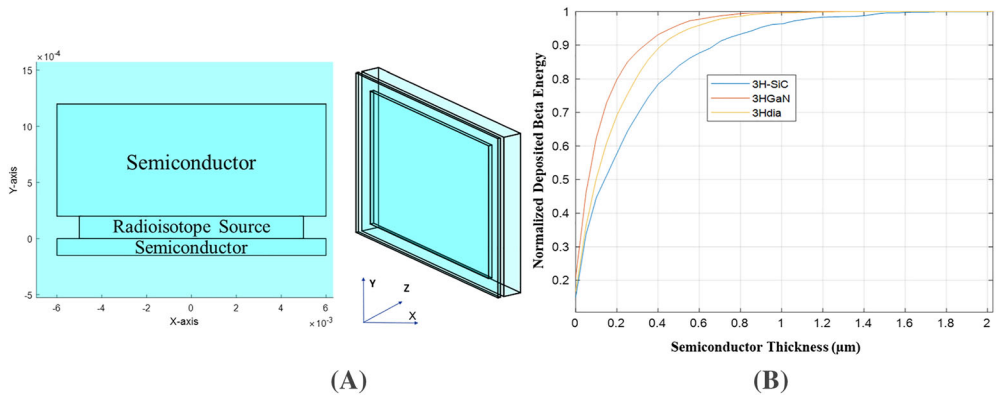

FIGURE 5 A, Illustration of the planar configuration and B, graph of the normalized deposited beta energy as function of semiconductor thickness. The planar coupling configuration is the surface interface between the radioisotope source and semiconductor [Colour figure can be viewed at wileyonlinelibrary.com]

P_{β^-} of a single textured feature unit cell. Parameters measured and calculated in the planar configuration were repeated in the 3-D configuration. In addition, the 1-cm^3 nuclear-battery calculations were repeated in the 3-D configuration with 1-μm and 100-μm semiconductor thicknesses.

3 | RESULTS

3.1 | Planar (2-D) coupling configuration results

Relative error of all simulations was less than 0.10, producing reliable statistics when using a cylindrical, volumetric source.[33] Nearly all of the β^- energy was deposited within 1.5 μm of the 4H-SiC disk on each side for all tritiated nitroxide thicknesses (D_L = 500 nm to 20 μm). The β^- source efficiencies for each D_L were fit to a rational function (Figure 6). Overall, the tritiated nitroxide compounds (C401, C30175, etc) have the highest η_β beginning at 100 nm. Also, the tritiated nitroxide compounds (i.e., C401) with lower mass densities within the group described in Table 2 have higher η_β. All tritiated nitroxides have $\eta_\beta >$ 30% when $D_L < 1\,\mu m$, which is nearly 20% higher than both titanium tritides from 100 $nm \le D_L < 1\,\mu m$.

Based on the η_β curve fits for each tritiated compound, the S_m and P_{β^-} were calculated and plotted following Section 2.2 formulation (Figure 7A). To confirm model accuracy within the research community, the Ti^3H_2 and $Ti^3H_{1.6}$ MCNP6 models' $D_{0.99}$, $P_{\beta^-}(D_{0.99})$, and P_{β^-} as a function of the D_L curve were compared with previously published results from Kavetsky et al,[25] Thomas et al,[4] and Alam et al.[7] The Ti^3H_2 model curve was compared with the point β^- source dose function for thin-layer sources, which is an empirically based function (Figure 7B).[20] The percent error between both curves is very large, from 0.1 μm to 0.5 μm, but decreases from 4.16% as the Ti^3H_2 layer increases from 1 μm. The $P_{\beta^-}(D_{opt})$ and $P_{\beta^-}(D_{0.99})$ percent errors between the empirical function and numerical model were approximately 3.78% and approximately 1.65%, respectively. The $Ti^3H_{1.6}$ model was compared with titanium tritide experimental data (Figure 7B). The $P_{\beta^-}(D_L = 400\ nm)$ percent error between experimental results from Thomas et al and our numerical model was 1.12%. The Ti^3H_2 model was compared with another titanium tritide numerical method from Alam et al (Figure 7B). The $P_{\beta^-}(D_L = 400\ nm)$ percent difference between Alam et al[7] and our numerical model was 5.82%. The percent difference of the η_β between both models was 5.80%.

Only one tritiated nitroxide, C409, has a greater P_{β^-} than $Ti^3H_{1.6}$ and Ti^3H_2 when $D_L \ge 300\ nm$ and $D_L \ge 500\ nm$, respectively. For example, the C409 is 26.8% and 55% greater than Ti^3H_2 and $Ti^3H_{1.6}$, respectively, when $D_L = 1\ \mu m$. For the 1-cm^3 nuclear battery, the electrical power density ($P_{e,vol}$) was calculated for each tritiated compound as a function of radioisotope layer thickness (D_L), as shown in Figure 8. The η_s used to calculate $P_{e,vol}$ was 18.6% because the majority of β^- energy was deposited within 1.5 μm of the 4H-SiC disk on each side for all tritiated nitroxide thicknesses (D_L = 100 nm to 20 μm).[4] This is within the depletion-region width; thus, the collection efficiency is unity. Two different semiconductor thicknesses (1 and 100 μm) were used (Figure 3 in Section 2.2). Table 3 shows the V_m and number of source and converter layers at the D_L that produce the maximum $P_{e,vol}$. In addition, the $P_{e,vol}$ at D_{opt} and $D_{0.99}$ are shown in Table 3.

The results of the 1-cm^3 nuclear battery using Ti^3H_2 with 1-μm thick 4H-SiC layers were compared with the Alam et al Ti^3H_2 results (Table 4). The percent difference between our results and the Alam et al results, using their approach,[7] was 3.21% at D_L = 300 nm. The percent

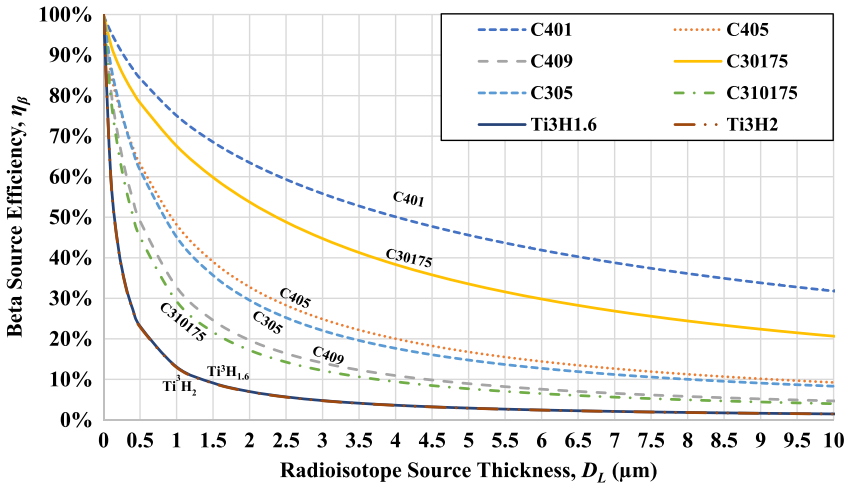

FIGURE 6 Graph of beta-source efficiency (η_β) as a function of radioisotope-source thickness (D_L). All tritiated nitroxides have higher beta-source efficiency than titanium tritides [Colour figure can be viewed at wileyonlinelibrary.com]

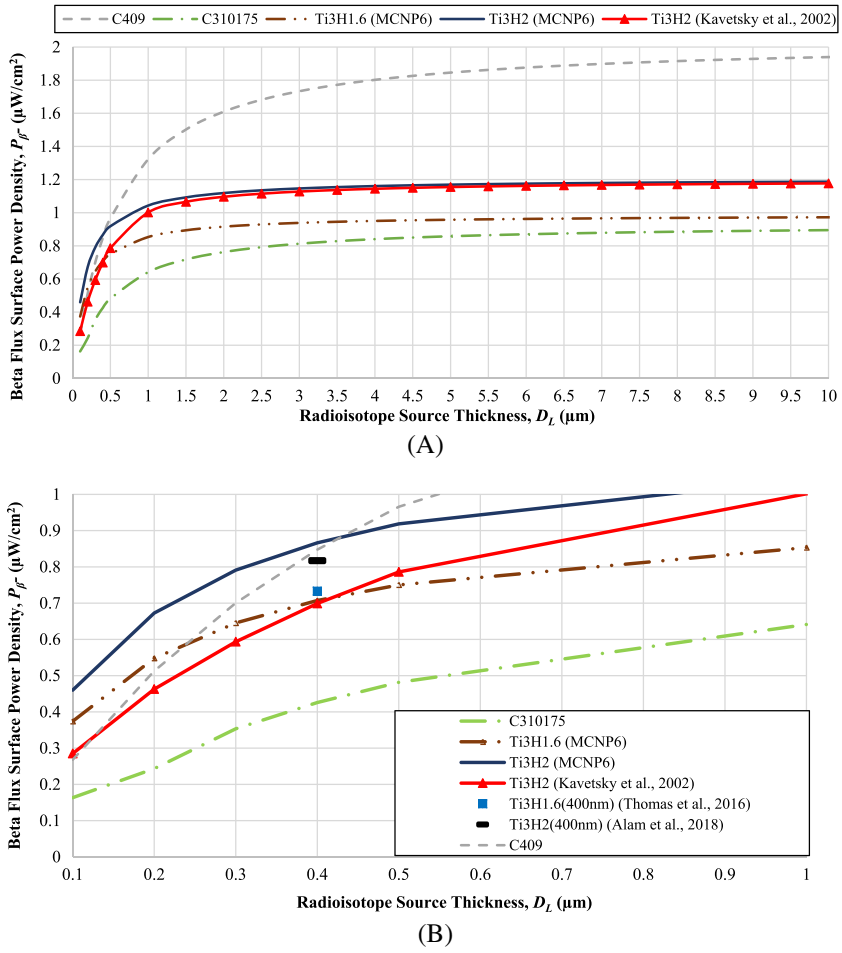

FIGURE 7 Graphs of the beta surface power density (P_{β^-}) as a function of radioisotope-source thickness (D_L). C409 was the only tritiated nitroxide with a higher P_{β^-} than all simulated titanium tritides. Graph *A* shows the P_{β^-} from 100 nm to 10 μm; graph B show the P_{β^-} from 100 nm to 1 μm [Colour figure can be viewed at wileyonlinelibrary.com]

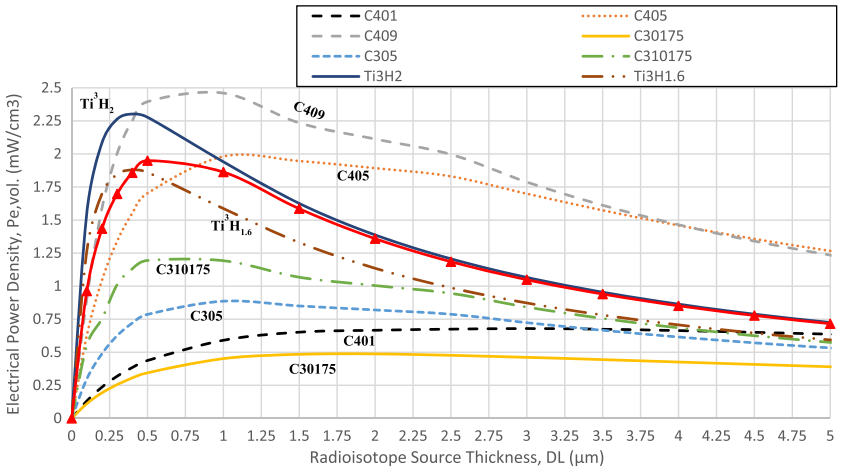

FIGURE 8 Graph of electrical power density or volumetric power output $(P_{e,vol})$ as a function of radioisotope-source thickness (D_L) [Colour figure can be viewed at wileyonlinelibrary.com]

difference between maximum $P_{e,vol}$ of both numerical methods, our model and the Alam et al[7] model, was 4.50% at two different D_L: 400 nm and 300 nm, respectively (Table 4).

The D_L where the $P_{e,vol}$ is maximum for both 4H-SiC layer thicknesses (1 and 100 μm) is not always equal to the D_{opt} or $D_{0.99}$ (Table 2). This assessment of tritiated compounds with 4H-SiC layers (1 and 100 μm) shows evidence in which D_{opt} and $D_{0.99}$ parameters are not as important when designing a 1-cm^3 nuclear battery using the planar, stacked-configuration approach (Table 5). Nevertheless, these parameters can still be considered vital when designing a single nuclear-battery packet, radioisotope source between two semiconductor converters, where the footprint area rather than volume is the nuclear battery's application constraint.

TABLE 3 Maximum electrical power density ($P_{e,vol}$) characteristics for all simulated tritiated compounds in planar, stacked configuration for 1-cm^3 nuclear battery; the η_s is 18.6%

	Max $P_{e,vol}$ (D_L, η_β) [mW/cm^3], η_s = 18.6%		Number of Radioisotope and Converter Layers		V_m [Ci/cm^3]	
4H-SiC layer	1 μm	100 μm	1 μm	100 μm	1 μm	100 μm
C401	0.68(2.5 μm, 59%)	0.058(29 μm, 15%)	2857	78	133	41
C405	1.98(1 μm, 48%)	0.072(11 μm, 8.5%)	5000	90	559	92
C409	2.46(1 μm, 33%)	0.066(7.5 μm, 6%)	5000	93	838	117
C30175	0.487(2 μm, 54%)	0.028(17.5 μm, 13%)	3333	85	104	23
C305	0.887(1 μm, 45%)	0.0308(10 μm, 8.32%)	5000	91	222	40
C310175	1.19(0.5 μm, 45%)	0.0306(6.5 μm, 6%)	6666	94	302	55
$Ti^3H_{1.6}$	1.88(0.4 μm, 27.30%)	0.034(4 μm, 3.63%)	7142	96	764	103
Ti^3H_2	2.3(0.4 μm, 27.09%)	0.042(4 μm, 3.59%)	7142	96	944	127

TABLE 4 A characteristic comparison between two different numerical methods for fully tritiated titanium tritide (Ti^3H_2)

	4H-SiC layer	$P_{e,vol}$ (D_L) [mW/cm^3] 1 μm	Number of Radioisotope and Converter Layers 1 μm
MCNP6	Ti^3H_2	3.16(300 nm)	7692
MCNP6	Ti^3H_2	3.22(400 nm)	7142
Alam et al[7]	Ti^3H_2	3.06(300 nm)	7691

Note. The Alam et al[7] approach was to calculate the $P_{e,vol}$ (D_L) from our MCNP6 results for comparison.

TABLE 5 Electrical power density ($P_{e,vol}$) at $D_{0.99}$ and D_{opt} for all simulated tritiated compounds in planar, stacked configuration for 1-cm^3 nuclear battery

	$P_{e,vol}$($D_{0.99}$, η_β) [mW/cm^3], η_s = 18.6%		$P_{e,vol}$ (D_{opt}, η_β) [mW/cm^3], η_s = 18.6%	
4H-SiC layer	1 μm	100 μm	1 μm	100 μm
C401	0.36(17 μm, 22%)	0.0554(17 μm, 22%)	0.561(7 μm, 39%)	0.0419(7 μm, 39%)
C405	0.896(7.5 μm, 11.9%)	0.0708(7.5 μm, 11.9%)	1.98(1 μm, 48.2%)	0.0197(1 μm, 48.2%)
C409	1.14(5 μm, 9%)	0.0654(5 μm, 9%)	2.4(0.5 μm, 49%)	0.0358(0.5 μm, 49%)
C30175	0.243(11.5 μm, 18.5%)	0.0272(11.5 μm, 18.5%)	0.462(3 μm, 44.7%)	0.0179(3 μm, 44.7%)
C305	0.347(8.5 μm, 9.5%)	0.0304(8.5 μm, 9.5%)	0.887(1 μm, 45.1%)	0.0176(1 μm, 45.1%)
C310175	0.532(5 μm, 7.7%)	0.0305(5 μm, 7.7%)	1.19(0.5 μm, 45%)	0.0178(0.5 μm, 45%)
$Ti^3H_{1.6}$	0.872(3 μm, 4.78%)	0.034(3 μm, 4.78%)	1.70(0.2 μm, 42.8%)	0.0203(0.2 μm, 42.8%)
Ti^3H_2	1.06(3 μm, 4.73%)	0.0414(3 μm, 4.73%)	2.09(0.2 μm, 42.6%)	0.025(0.2 μm, 42.6%)

Note. The η_s is 18.6% (refer to Table 3 for $P_{e,vol}$ comparison).

Tritiated nitroxide C4 at all three densities (0.1, 0.5, and 0.9 g/cm^3) has a greater $P_{e,vol}$ than $Ti^3H_{1.6}$ and Ti^3H_2 based on a 100-μm-thick 4H-SiC layer. However, only C409 has a greater $P_{e,vol}$ than $Ti^3H_{1.6}$ and Ti^3H_2, based on a 1-μm-thick 4H-SiC layer. These different outcomes are solely caused by the different 4H-SiC layer thicknesses. The 100-μm-thick 4H-SiC layers make up the majority of the 1-cm^3 nuclear-battery volume compared with the radioisotope source, thus eliminating the titanium tritide's thinner layer advantage over all but one tritiated nitroxide. With the 1-μm 4H-SiC layers, the thickness proportion of the source and converter is much closer, where they are nearly equal in volume percentage of the 1-cm^3 nuclear battery. C305 and C405 have higher

$P_{e,vol}$ than C310175 and C409, respectively, using 100-μm-thick 4H-SiC layers because the η_β is higher with lower-density compounds. The results show this relationship only occurs when the source and converter thicknesses are an order of magnitude different. In addition, the V_m of tritiated nitroxide C4 (C401, C405, and C409) in the 1-cm^3 nuclear battery was lower than the $Ti^3H_{1.6}$ and Ti^3H_2 for both 4H-SiC thicknesses. The reasons for higher $P_{e,vol}$ with lower V_m were because of higher η_β and A_m for all three tritiated compounds (C401, C405, and C409).

3.2 | 3-D coupling configuration results

Tritiated nitroxide C4, specifically C405, was picked as the tritiated compound for all 3-D coupling configuration simulations. C409 has the highest P_{β^-} and $P_{e,vol}$ (1- and 100-μm-thick 4H-SiC layers) of all simulated compounds described in this paper. Most importantly, C401, C405, and C409 have a greater $P_{e,vol}$ than $Ti^3H_{1.6}$ and Ti^3H_2 based on 100-μm-thick 4H-SiC layers, which can currently be produced with the Smart Cut (also Smart cut or Smart-Cut) process.[23,24] C405 was picked as the simulated tritiated compound because its bulk density of 0.5 g/cm^3 is close to the experimental bulk-density range of approximately 0.27 to 0.76 g/cm^3 when deposited on Si rectangular-pillar array surface, respectively (Figures 9 and 10).[34] The top radioisotope layer thickness was set constant at 1 μm, the thickness of the maximum $P_{e,vol}$ of planar coupling configuration with 1-μm-thick 4H-SiC layers. Also, this is the D_{opt} of C405.

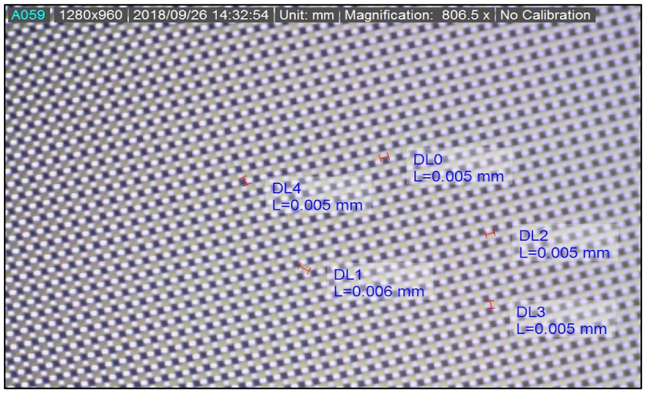

FIGURE 9 Microscope camera's top-view image at 806.5× magnification of Si rectangular-pillar array. The etched depth (***d***) is 10.8 μm. The feature width (***w***) and gap for the radioisotope source (***a***) are 5 μm [Colour figure can be viewed at wileyonlinelibrary.com]

Relative error of all 3-D simulations was less than 0.10. The η_β with and without the top radioisotope source layer as a function of $\boldsymbol{a}$ were fit to rational functions (Figure 11). The rectangular, cylindrical, and hexagonal arrays' average η_β from 100 $nm \leq \boldsymbol{a} \leq 10\ \mu m$ was 11% higher than planar-configuration η_β from 100 $nm \leq D_L \leq 10\ \mu m$. On average, ridge-array η_β from 100 $nm \leq \boldsymbol{a} \leq 10\ \mu m$ was 2% higher than the planar-configuration η_β from 100 $nm \leq D_L \leq 10\ \mu m$. The rectangular-pillar array was the only 3-D coupling configuration with a lower η_β than the planar coupling for the entire $\boldsymbol{a}$ range when excluding the top radioisotope-source layer. When the top radioisotope-source layer was included, all 3-D coupling configurations have lower total η_β than the planar coupling configuration for the entire $\boldsymbol{a}$ range (Figure 12). The lower total beta-source efficiency is caused by the lower surface-area coupling between top source layer and top face of the textured surface array per 1 cm^2.

The S_m and P_{β^-} for unit cell array per 1 cm^2 were calculated using the η_β curve fits for each textured surface array

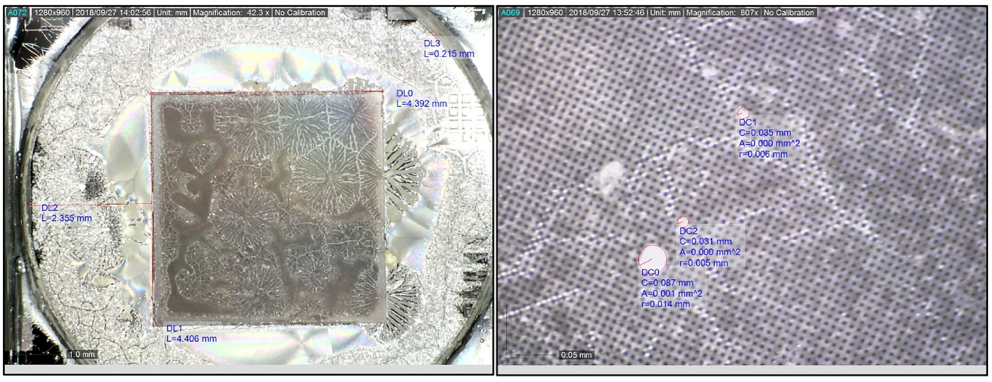

(A) **(B)**

FIGURE 10 Microscope camera's top-view images at (A) 42.3× and (B) 807× magnification of Si rectangular-pillar array. The hydrogenated nitroxide is translucent. A, The dark square is the Si rectangular-pillar array. A, The lighter area around the dark square is the Si planar surface. B, The nitroxide coating, using methyl ethyl ketone as the solvent, is relatively uniformly based on optical observation [Colour figure can be viewed at wileyonlinelibrary.com]

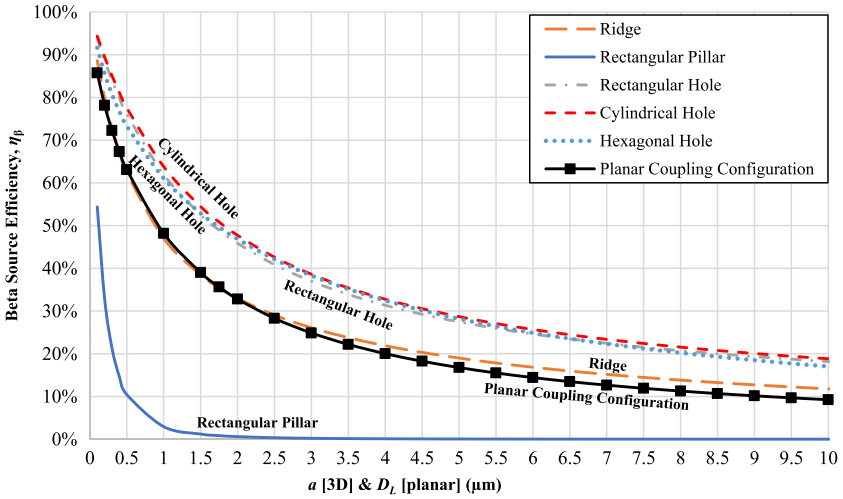

FIGURE 11 Graph of 3-D and planar coupling beta-source efficiency as a function of $\boldsymbol{a}$ (3-D configuration) and D_L (planar configuration) of C405, respectively, for which rectangular-pillar array has the lowest efficiency throughout the entire model range. The D_L axis is for the planar-coupling configuration and the $\boldsymbol{a}$ is for all textured surface arrays. The top radioisotope-source layer efficiency is excluded for 3-D coupling configuration beta-source efficiency [Colour figure can be viewed at wileyonlinelibrary.com]

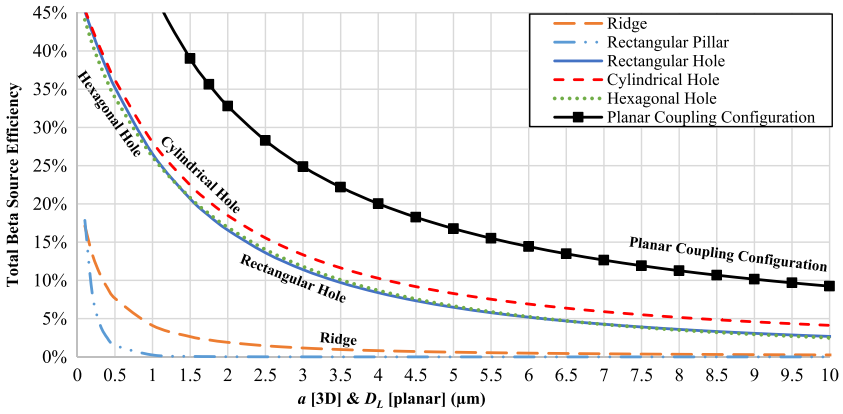

FIGURE 12 Graph of total beta-source efficiency as a function of $\boldsymbol{a}$ (3-D configuration) and D_L (planar configuration) of C405. For the 3-D configuration, the top radioisotope layer efficiency is included in the total beta-source efficiency. All 3-D configurations' total beta-source efficiencies are lower than planar-coupling configuration. The D_L axis is for the planar-coupling configuration and the $\boldsymbol{a}$ is for all textured surface arrays [Colour figure can be viewed at wileyonlinelibrary.com]

following the planar-coupling formulation. The rectangular-pillar array has the highest bidirectional beta-flux surface power activity ($2P_{\beta^-}$) of all of the 3-D and planar-coupling configurations at $\boldsymbol{a} = 500\ nm$ (Figure 13). The rectangular-pillar array's $2P_{\beta^-}$ increases by a factor of 5.9 at $\boldsymbol{a} = 500\ nm$ compared with the planar-coupling configuration at $D_{0.99} = 7\ \mu m$. As $\boldsymbol{a}$ increases, the 3-D-packet configuration with the highest $2P_{\beta^-}$ switches to the ridge array from $1.75\ \mu m \leq \boldsymbol{a} \leq 3.5\ \mu m$ and then, finally, cylindrical holes from $3.5\ \mu m \leq \boldsymbol{a} \leq 10\ \mu m$. Table 6 shows the $2P_{\beta^-}$ activity per 1-cm^2 packet footprint, factor of increase in $2P_{\beta^-}$ ($\boldsymbol{X}$), and η_β, excluding the top radioisotope-source layer, at the maximum $2P_{\beta^-}$ for each textured surface array compared with the planar-coupling configuration.

The textured surface arrays' $P_{e,vol}$ with 1- and 100-μm-thick 4H-SiC layers as a function of $\boldsymbol{a}$ nearly follows the same trend as the $2P_{\beta^-}$ of textured surface (Figures 14 and 15). The $P_{e,vol}$ was calculated through the same process as the planar-coupling configuration with a constant semiconductor-conversion efficiency of 18.6%.[4] The rectangular-pillar array has the highest $P_{e,vol}$ for both 1-cm^3 nuclear batteries (1- and 100-μm-thick 4H-SiC layers) compared with all simulated 3-D and planar-coupling configurations. The planar-coupling configuration has a higher $P_{e,vol}$ than the other four textured surfaces with 1-μm-thick 4H-SiC layers. The reasons for this surprising outcome are the lower total beta-source conversion efficiency due to lower surface-area coupling between the top radioisotope-source layer and textured surface semiconductor converter.

The textured surface feature's height lowers the amount of source and converter layers in the volume (Table 7). All simulated textured surface arrays have a higher $P_{e,vol}$ than planar-coupling configuration with 100-μm-thick 4H-SiC layers from $400\ nm \leq \boldsymbol{a} \leq 8.5\ \mu m$. This outcome is different than the previous one because a bulk of the volume is 4H-SiC. This stacked configuration has the textured surface features grown or etched from the 100-μm-thick 4H-SiC layers (Figure 16). Now, there is an increasing factor of $P_{e,vol}$ because of the increased, active surface-area coupling between the source and textured surface converters. Table 7 shows the maximum $P_{e,vol}$ (1- and 100-μm-thick 4H-SiC layers) and important parameters and results at the maximum

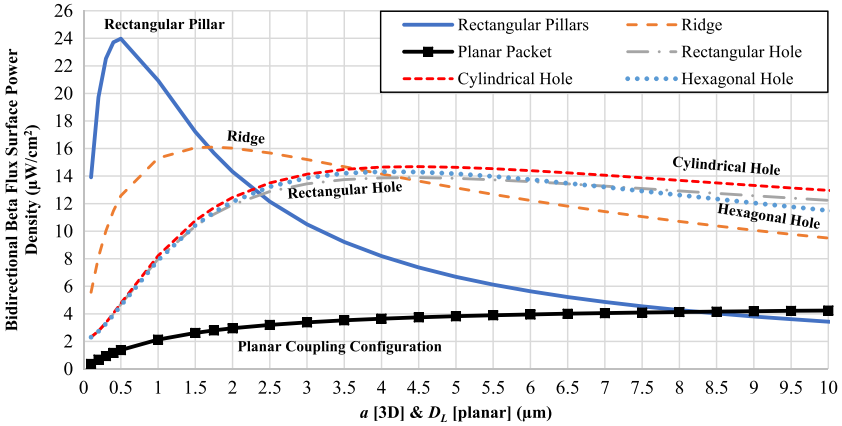

FIGURE 13 Graph of bidirectional beta-flux surface power density $(2P_{\beta^-})$ as a function of $\boldsymbol{a}$ (3-D coupling configuration) and D_L (planar configuration) of C405. The 3-D-packet and planar-packet configuration is the radioisotope source between two semiconductor converters. All textured surfaces except rectangular-pillar array have higher $2P_{\beta^-}$ than the planar-coupling configuration packet from $100\ nm \leq \boldsymbol{a} \leq 10\ \mu m$. The D_L axis is for the planar-coupling configuration and the $\boldsymbol{a}$ is for all textured surface arrays. The planar packet comprises of the radioisotope source between two semiconductor converters (transducers) [Colour figure can be viewed at wileyonlinelibrary.com]

TABLE 6 3-D-packet and planar-packet configuration parameters.

	$2P_{\beta^-}$ [μW/cm^2]	η_β	Activity per 1-cm^2 Packet Footprint (Ci)	X
Rectangular pillar	24 (a = 0.5 μm)	1.51%	1.44	5.9
Ridge	16.1 (a = 1.75 μm)	2.22%	1.22	4.0
Rectangular hole	13.9 (a = 4.5 μm)	7.34%	1.26	3.4
Cylindrical hole	14.7 (a = 4.5 μm)	9.2%	1.26	3.6
Hexagonal hole	14.3 (a = 4 μm)	8.7%	1.17	3.5
Planar coupling configuration	4.05 ($D_{0.99}$ = 7 μm)	12.7%	0.83	1

Note. A packet is defined as a radioisotope source layer between two semiconductor converters. The 3-D-packet configuration η_β excludes the top source layer in the calculation.

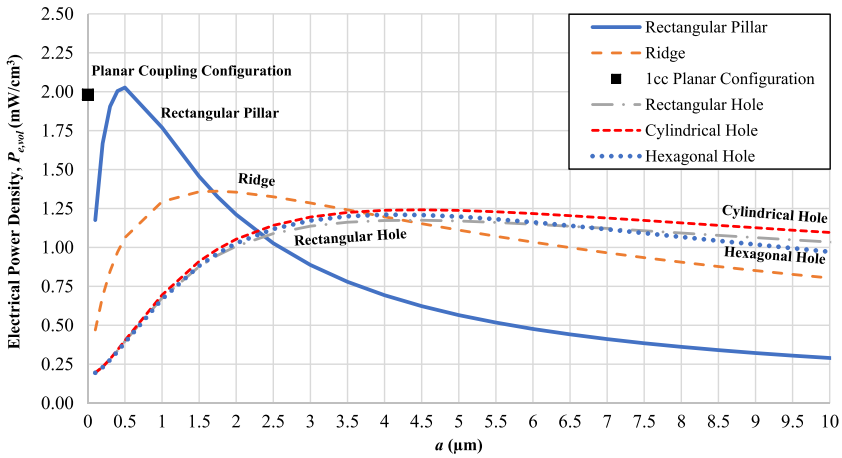

FIGURE 14 Graph of electrical power density ($P_{e,vol}$) as a function of $\boldsymbol{a}$ of C405 with 1-μm-thick 4H-SiC layers for 1-cm^3 nuclear battery. Rectangular-pillar array is the only textured surface array with a higher $P_{e,vol}$ than 1-cm^3 nuclear battery using planar-coupling configuration. For the 1-cm^3 (**1 cc**) planar-coupling configuration, the maximum electrical power density is at $\boldsymbol{D_L}$ of 1 μm and $\boldsymbol{a}$ is equal to 0 [Colour figure can be viewed at wileyonlinelibrary.com]

$P_{e,vol}$ (1- and 100-μm-thick 4H-SiC layers), including the planar-coupling configuration.

The two highest textured surface arrays' $P_{e,vol}$, for rectangular-pillar array at 2.02 mW/cm^3 and ridge array at 1.36 mW/cm^3, were further analyzed by changing $\boldsymbol{w}$ and $\boldsymbol{a}$. For the rectangular-pillar array, the $\boldsymbol{w}$ and $\boldsymbol{a}$ were equally changed; that is, $\boldsymbol{w}$ = 100 nm and $\boldsymbol{a}$ = 100 nm. The maximum $P_{e,vol}$ (1- and 100-μm-thick 4H-SiC layers) at $\boldsymbol{w}$ = 100 nm and $\boldsymbol{a}$ = 100 nm was more than double the previous rectangular-pillar array's $P_{e,vol}$ (1- and 100-μm-thick 4H-SiC layers), as graphed in Figure 17. For the ridge array, MCNP simulations of different $\boldsymbol{a}$ and $\boldsymbol{w}$ sets were run and analyzed to calculate $P_{e,vol}$ with 1-μm-thick 4H-SiC layers. A two-variable polynomial function (P_e,

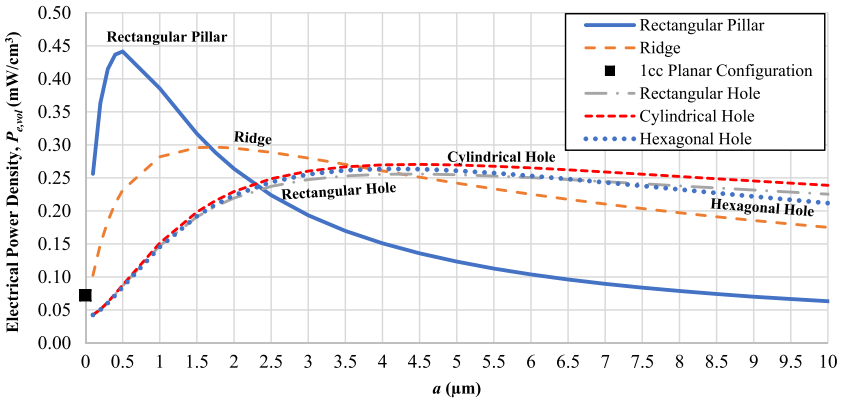

FIGURE 15 Graph of electrical power density ($P_{e,vol}$) as a function of $\boldsymbol{a}$ of C405 with 100-μm-thick 4H-SiC layers for 1-cm^3 nuclear battery. All textured surface arrays have higher $P_{e,vol}$ than 1-cm^3 nuclear battery using planar-coupling configuration from 400 $nm \leq \boldsymbol{a} \leq 8.5\ \mu m$. Rectangular-pillar array has the highest $P_{e,vol}$. For the 1-cm^3 (*1 cc*) planar-coupling configuration, the maximum electrical power density is at $D_L = 11$ μm and $\boldsymbol{a}$ is equal to 0 [Colour figure can be viewed at wileyonlinelibrary.com]

TABLE 7 textured1-cm^3 nuclear-battery 3-D coupling configuration characteristics at the maximum $P_{e,vol}$ of C405 compared with planar coupling configuration

	Max $P_{e,vol}$(a, η_β, X) [mW/cm^3]		Number of Radioisotope and Converter Layers		V_m [Ci/cm^3]	
4H-SiC layer	**1 μm**	**100 μm**	**1 μm**	**100 μm**	**1 μm**	**100 μm**
Rectangular pillar	2.03(0.5 μm, 1.5%, 1.02)	0.441(0.5 μm, 1.5%, 6.13)	454	99	633	138
Ridge	1.36(1.75 μm, 2.22%, 0.687)	0.297(1.75 μm, 2.22%, 4.12)	454	99	557	121
Rectangular hole	1.17(4.5 μm, 7.3%, 0.59)	0.256(4.5 μm, 7.3%, 3.55)	454	99	571	124
Cylindrical hole	1.24(4.5 μm, 9.2%, 0.627)	0.27(4.5 μm, 9.2%, 3.76)	454	99	571	124
Hexagonal hole	1.21(4 μm, 8.7%, 0.611)	0.264(4 μm, 8.7%, 3.66)	454	99	533	116
Planar coupling configuration	1.98(1 μm, 48.17%, 1)	0.0718(11 μm, 8.49%, 1)	5000	87	559	92.3

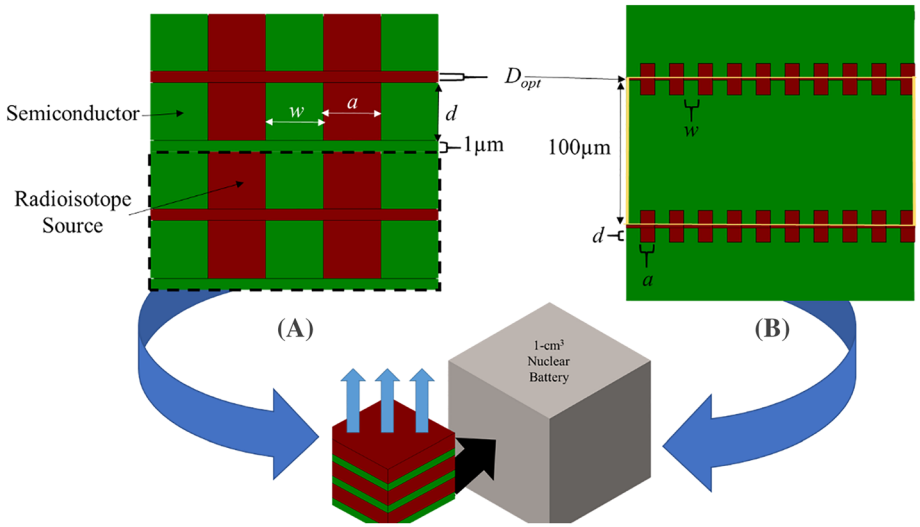

FIGURE 16 Illustrations of the 3-D coupling, (A) stacked configuration for a 1-cm^3 nuclear battery with either 1- or (B) 100-μm-thick 4H-SiC layers. (A) The portions enclosed by either the black dashed line or (B) yellow solid line are repeated and stacked to reach a 1-cm thickness by 1 cm^2. Illustrations are not drawn to scale [Colour figure can be viewed at wileyonlinelibrary.com]

$_{vol}(\boldsymbol{w},\boldsymbol{a})$) was fit to the results, generating a surface and contour plot (Figure 18). The global maximum $P_{e,vol}$ (1-μm-thick 4H-SiC layers) is $2.67\frac{mW}{cm^3}$, where the $\boldsymbol{w}$ and $\boldsymbol{a}$ are 100 nm, which is the minimum limit with the curve fit. The global minimum of the surface plot was $0.746(876\ nm, 420\ nm)\frac{mW}{cm^3}$; the local maximum of the

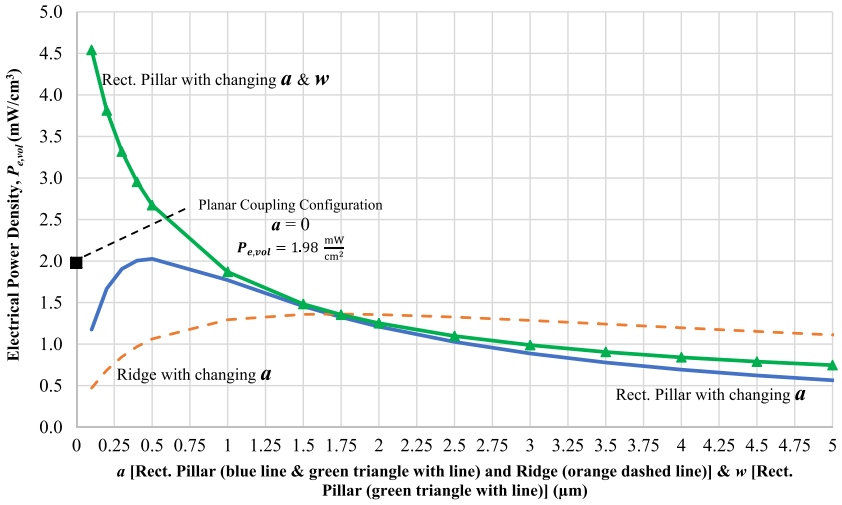

FIGURE 17 3-D coupling configuration's electrical power density as a function of feature size comparing different pillar arrays with ridge array with 1-μm-thick 4H-SiC layers. For rectanglar pillar arrays with changing w and a, the x-axis is both w and a since they are changing at the same rate. For the 1-cm^3 (*1 cc*) planar-coupling configuration, a is equal to 0 [Colour figure can be viewed at wileyonlinelibrary.com]

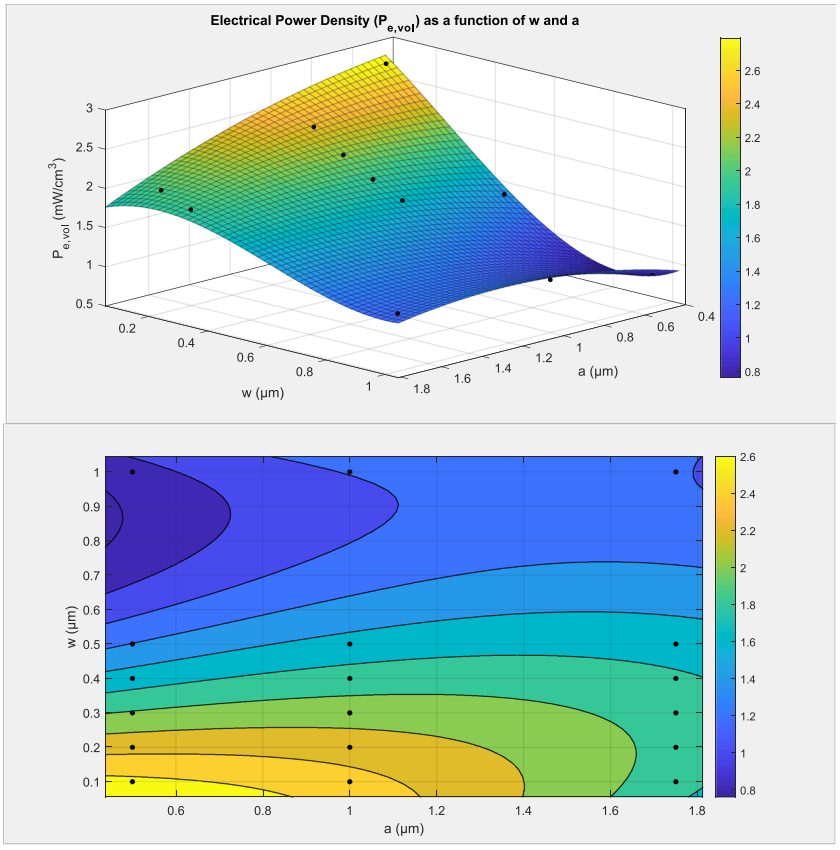

FIGURE 18 Surface and contour plot of electrical power density ($P_{e,vol}$) as function of w and a for ridge array with 1-μm-thick 4H-SiC layers. The w and a are the semiconductor converter feature's width and radioisotope-source width, respectively. The depth of the semiconductor features (d) is constant at 10 μm. The solid black points are calculated points from numerical method [Colour figure can be viewed at wileyonlinelibrary.com]

surface plot was $1.919(243\ nm, 1.77\ \mu m)\frac{mW}{cm^3}$. The results of both arrays dispute the initial MCNP simulation to identify the optimal 4H-SiC feature's width thickness (w) that will absorb 95% of the normalized beta energy, 1 μm. Based on our numerical method, the textured surface array results demonstrate that a thinner and more equivalent w and a produce a higher $P_{e,vol}$ with C405 as the radioisotope source. Source and transducer coupling shifts from planar-surface interface toward a volume interface with thinner and more frequent features (textured surface transducer and radioisotope source gap) per area.

4 | DISCUSSION

Our numerical method results of the planar-coupling configuration reveal that certain characteristics have more impact than others when designing a 1-cm^3 βV nuclear battery. For example, D_{opt} and $D_{0.99}$ are important parameters for beta-flux surface power density (P_{β^-}) but not the

maximum electrical power density ($P_{e,vol}$) with 1- and 100-μm-thick 4H-SiC layers. The radioisotope layer thickness is different at these maximum points. C401, C405, and C409 have the highest $P_{e,vol}$ with 100-μm-thick 4H-SiC layers. Additionally, all but one of the tritiated nitroxide nuclear batteries—C409 with 1- and 100-μm-thick 4H-SiC layers—contain less activity per 1 cm^3 than the titanium tritide nuclear batteries (Table 3). Once C4 tritiation is successful and stable with negligible $^3H_2$ loss, we will be able to build a ^{3}H-based βV nuclear battery that is equal or greater in $P_{e,vol}$ to all previous ^{3}H-based prototypes using less $^3H_2$ per volume. The planar-coupling configuration results identified the tritiated compound with highest $P_{e,vol}$ from the simulated compounds. These conclusions are from a numerical method with percent differences of less than 6% when comparing Ti^3H_x results with previous empirical and numerical methods' results.

Tritiated nitroxides (C3 and C4) have higher beta-source efficiencies than the titanium tritides because of lower mass densities. In general, a low-mass-density-tritiated compound increases beta-source efficiency (η_β) but, at the same instance, reduces the activity per unit volume (V_m), thus lowering the $P_{e,vol}$. This relationship is demonstrated when the semiconductor-converter thickness is nearly proportional to the radioisotope-source thickness. This is the most ideal case for βV nuclear batteries in which a source-depositing and converter-stacking process can be applied and the source volume (V_S) and converter volume (V_C) ratio $\left(\frac{V_S}{V_C}\right)$ is proportional. With a volume of 1 cm^3 made of 1-μm-thick 4H-SiC layers, the number of source and converter layers decreases when the optimal source layers are thicker with a lower-mass-density compound (Table 3). C409 $\left(\rho_m = 0.9\frac{g}{cm^3}\right)$ was the only tritiated nitroxide with a higher beta-flux surface power density and $P_{e,vol}$ with 1-μm-thick 4H-SiC layers than the two titanium tritides. The source thickness was equal to the converter thickness, whereas the two titanium tritides' source thicknesses were less than half of the converter thickness. For C3 and C4, as the mass density increases with the same A_m, the source thickness (D_L) at the maximum $P_{e,vol}$ point decreases while the $P_{e,vol}$ increases (Figure 8). This relationship was provided with further evidence from simulated tritiated nitroxides at different bulk and particle densities, including densities that are presently unattainable with C4 (Figure 19). The manufacturable limit for our applications is the D_L at this maximum $P_{e,vol}$ point. Minimum coating thicknesses using a spin-coating method will need to be investigated with C4. Based on the curve fit of simulated data, the tritiated nitroxide C4 would require a minimum bulk density of 0.41 and 0.63 g/cm^3 to equal the $P_{e,vol}$ of $Ti^3H_{1.6}$ (negligible $^3H_2$ loss) and Ti^3H_2 (unstable, significant $^3H_2$ loss), respectively.

Tritiated nitroxide C405 was selected because its bulk density is the closest to the actual deposited coatings with a similar hydrogenated nitroxide on planar and textured surfaces. Finally, this compound has already been fully deuterated and stable, making it one step away from tritiation.[26] The decision to select certain textured surface arrays for simulations is backed by conceivable fabrication, etching, and growth of these textured surfaces. The unit cell array's beta-source efficiency was higher for most 3-D coupling configurations. Intuitively, if the surface-area coupling between the source and converter is increased so more surfaces are interfacing with each other, the percentage of deposited beta energy into the converter volume will increase, thus increasing η_β. The rectangular-pillar array was the only 3-D coupling configuration with a lower beta-source efficiency because the surface-area coupling was the lowest between the source and converter. There was more radioisotope source with thinner textured surface feature widths producing an overall lower η_β relative to the other feature types (Figure 11 and 12). When the top-layer radioisotope source is included, the total η_β is less than the planar-coupling configuration for all simulated textured surface arrays. The reason for this outcome is the lack of surface-area coupling with the top-source layer and top face of textured surface array. The percentage of deposited beta energy in the converter base from the top-source layer is close to zero. The tritium beta energy is

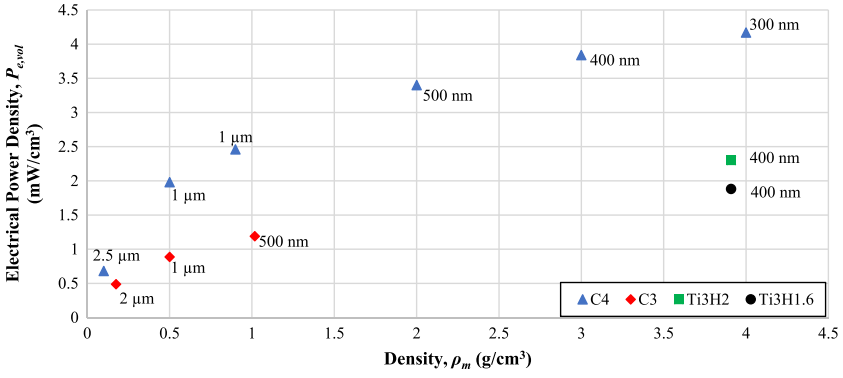

FIGURE 19 Graph of electrical power density as function of C4 and C3 densities compared with titanium tritide. For C4 and C3, as the mass density (ρ_m) increases, the maximum electrical power density increases while the radioisotope-source thickness (D_L, labeled near each point) at maximum electrical power density point decreases [Colour figure can be viewed at wileyonlinelibrary.com]

not high enough to pass through 10 μm of C405 and deposit into the 4H-SiC base. A final design decision should prioritize either higher η_β or maximizing $P_{e,vol}$ in the 1-cm^3 nuclear battery.

The bidirectional surface power density per 1 cm^2 $\left(2P_{\beta^-}\right)$ of all textured surface arrays was higher than the planar-coupling configuration's $2P_{\beta^-}$. The rectangular-pillar array has the highest $2P_{\beta^-}$ at $w = 1\ \mu m$ and $\boldsymbol{a} = 500\ nm$ with a factor of 5.9 compared with planar-coupling configuration. The maximum $2P_{\beta^-}$ switches to different textured surface feature types as the $\boldsymbol{a}$ increases. The order of $2P_{\beta^-}$ maximum switching from each feature type to another is dependent on the rate of decreasing total η_β as a function of $\boldsymbol{a}$. The textured surface arrays' $P_{e,vol}$ as a function of $\boldsymbol{a}$ follows the $2P_{\beta^-}$ trend with 1- and 100-μm-thick 4H-SiC layers. Only the rectangular-pillar array has a higher $P_{e,vol}$ than planar-coupling configuration in which both configurations are using 1-μm-thick 4H-SiC layers. Furthermore, the rectangular-pillar array uses 13% more tritium activity than the planar-coupling configuration. This enlightening result contradicts an obvious premise that more surface-area coupling increases electrical power density for all cases. It, also, depends on how efficiently the beta particles from the core of the radioisotope source can reach the semiconductor's collection region. The lower total η_β and V_m are the reasons for the reduction of electrical power density with some of the 3-D coupling configurations. Moreover, textured surface feature and radioisotope source height reduce the number of source and converter layers in the 1-cm^3 volume. This relationship is similar to the planar-coupling configuration using 1-μm-thick 4H-SiC layers. The textured surface arrays' $P_{e,vol}$ with 100-μm-thick 4H-SiC layers were higher than planar-coupling configuration from $100\ nm \le \boldsymbol{a} \le 10\ \mu m$. This outcome is similar to the planar-coupling configuration with 100-μm-thick 4H-SiC layers for that the converter base thickness is most of the 1-cm^3 volume, so the thicker radioisotope layers or textured feature height of 10 μm are now a small fraction of the total volume. The 3-D surface-area coupling advantages are now the dominating factors with the $P_{e,vol}$ of the 1-cm^3 nuclear battery with 100-μm-thick 4H-SiC layers.

The planar and 3-D coupling configurations' figure of merit is $P_{e,vol}$. For the 3-D coupling configuration, a direct relationship between $P_{e,vol}$ and the ratio of the radioisotope source and converter volume $\left(\frac{V_S}{V_C}\right)$ was recognized for that the feature width ($\boldsymbol{w}$) and 4H-SiC layers' thickness are 1 μm. The array type with the highest $P_{e,vol}$ has the highest $\frac{V_S}{V_C}$ (Table 7). However, this direct relationship does not continue if the $\boldsymbol{w}$ changes, which was shown with further simulations of rectangular-pillar and ridge arrays. The rectangular-pillar array has the highest $P_{e,vol}$ and $\frac{V_S}{V_C}$, but the ridge array has a higher $P_{e,vol}$ and lower $\frac{V_S}{V_C}$ compared with the previous textured surface arrays with a constant $\boldsymbol{w}$ of 1 μm. When analyzing the results, maximizing activity per unit volume (V_m) does not always maximize the $2P_{\beta^-}$ and $P_{e,vol}$ as shown in Tables 6–8. Alam et al showed that low-mass-density materials increase the η_β but do not necessarily increase the electrical power density as the low-mass-density materials can store less tritium.[7] The converter's surface area ($S.A._C$) and volume (V_C) ratio $\left(\frac{S.A._C}{V_C}\right)$ show a partial, direct relationship with its $P_{e,vol}$ (Table 8). This relationship is inconclusive because of the whole arrays' results. Unfortunately, there is not one equation or variable to solve for to identify optimal textured surface array and its dimensions with a tritiated nitroxide source. The system has too many variables that

TABLE 8 3-D coupling configuration characteristics at the maximum $P_{e,vol}$ for a 1-cm^3 nuclear-battery

4H-SiC layer	max. $P_{e,vol}$ [mW/cm^3] 1 μm	V_m [Ci/cm^3] 1 μm	$\frac{V_S}{V_C}$ 1 μm	$\frac{S.A._C}{V_C}$ [μm^{-1}] 1 μm
Rectangular pillar, w = 0.1 μm, a = 0.1 μm	4.54	863	1.74	28.86
Rectangular pillar, w = 1 μm, a = 0.1 μm	2.03	633	1.204	3.67
Ridge, w = 0.1 μm, a = 0.1 μm	2.67	413	0.565	9.67
Ridge, w = 1 μm, a = 1.75 μm	1.36	557	0.977	1.09
Rectangular hole, w = 1 μm, a = 4.5 μm	1.17	571	0.933	0.847
Cylindrical hole, w = 1 μm, a = 4.5 μm	1.24	571	0.933	0.847
Hexagonal hole, w = 1 μm, a = 4 μm	1.21	533	0.831	0.0.915

Note. The 4H-SiC layer thickness is 1 μm.

require simulations and analysis to identify optimal textured surface feature type and dimensions when using the tritiated nitroxide as the radioisotope source.

5 | CONCLUSION

We find value in optimizing planar and 3-D coupling configurations to maximize the electrical power density (electrical power output per unit volume, $P_{e,vol}$) with solid tritium sources and the 4H-SiC βV cell. For the planar coupling configuration, the tritiated nitroxides have higher beta source efficiencies because of a lower mass density than the titanium tritide. However, because of lower mass density, most of them have lower activity per unit volume (V_m) than the titanium tritides. A tritiated nitroxide with a minimum density of 0.41 g/cm^3 at a A_m of 2372 (ie, C4) would generate a comparable $P_{e,vol}$ with the $Ti^3H_{1.6}$-based nuclear battery. When comparing the 3-D and planar coupling configuration, if the converter thickness is proportional or equal to D_L, $P_{e,vol}$ increase is narrowed or negligible, lessening the textured surface converter's main advantage over planar, conventional converters. On a practical standpoint based on the Smart Cut process improvement, it might be more feasible to produce 1-cm^3 using the planar configuration to reach milliwatt power levels with solid tritium sources. For example, Myers-Ward et al demonstrated an epitaxially grown unintentionally and nitrogen-doped 4H-SiC layer that was approximately 300 to 500 nm thick with an area of 50 × 50 μm^2 using the Smart Cut process.[35]

One of two untested parameters associated with current and future experimental and manufacturing limitations is the gap or width among the textured surface features' ($\boldsymbol{a}$); the other untested parameter is the experimental proof of tritiated nitroxide C4. Although there is not a published, experimental example of a textured surface 4H-SiC βV cells, there are examples of textured surface Si βV cells such as cylindrical holes.[12,36] The cylindrical-hole dimensions were approximately $0.84 \leq \boldsymbol{a} \leq 1\ \mu m$ and $10 \leq \boldsymbol{a} \leq 43\ \mu m$.[12,36] As stated before, C4 was successfully and fully deuterated while being stable. Still, the simulations of the 3-D coupling configuration with C405 identified the optimal 3-D array and its dimensions with a tritiated nitroxide. The η_β and $P_{e,vol}$ did increase as the source and transducer interface shifted closer to volume interface from a planar, surface interface for which the features ($\boldsymbol{w}$ and $\boldsymbol{a}$) are thinner and more frequent over 1-cm^2. Our numerical-method results and analysis of the planar and 3-D coupling configuration answered several questions toward designing a βV nuclear battery composed of a tritiated compound and 4H-SiC semiconductor-converter layers. These answers and discoveries are accurate with tritium and 4H-SiC based on the low percent errors and differences among previous experimental, empirical, and numerical results. Optimal dimensions and certain characteristics of planar and 3-D coupling configuration would be considerably different when using promethium-147 (higher β^- energy emission) and GaN (higher mass density than 4H-SiC). Nonetheless, relative to the tritium βV nuclear battery, our numerical method introduced new questions that would require further modeling and analysis, influenced by this described process, followed by experimental data to develop valid conclusions and correlations.

ACKNOWLEDGEMENTS

The authors wish to acknowledge NASA for sponsoring this research work, which will potentially lead to future RPSs on low-Earth-orbit and planetary CubeSat missions.

ORCID

Johnny Russo https://orcid.org/0000-0002-3421-8871
Tariq Rizvi Alam https://orcid.org/0000-0003-1074-1489

REFERENCES

1. Romer M. Ragone plot comparison of radioisotope cells and the direct sodium borohydride/hydrogen peroxide fuel cell with chemical batteries. *IEEE Trans Energy Convers*. 2008;23(1):171-178.
2. Prelas M, Boraas M, De La Torre Aguilar F, Seelig J, Tchakoua Tchouaso M, Wisniewski D. *Nuclear Batteries and Radioisotopes*. Switzerland: Springer International Publishing; 2016.
3. Bower KE, Barbanel YA, Shreter YG. *Polymers, phosphors, and voltaics for radioisotope microbatteries*. Boca Raton (USA): CRC Press; 2002.
4. Thomas C, Portnoff S, Spencer MG. High efficiency 4H-SiC betavoltaic power sources using tritium radioisotope. *Appl Phys Lett*. 2016;108(1):013505.
5. Liu Y, Tang X, Xu Z, et al. Influences of planar source thickness on betavoltaics with different semiconductors. *J Radioanal Nucl Chem*. 2015;304(2):517-525.
6. Moghissi A. A. and Carter M. W.. Tritium. Oak Ridge, TN: Oak Ridge National Laboratory, 1975.
7. Alam TR, Spencer MG, Prelas MA, Pierson MA. Design and optimization of radioisotope sources for betavoltaic batteries. *Int J Energy Res*. 2018;1-10.
8. Zhang L, Cheng H, Hu X, Xu X. Model and optimal design of ^{147}Pm SiC-based betavoltaic cell. *Superlattice Microst*. 2018;123:60-70.
9. Rahmani F, Khosravinia H. Optimization of silicon parameters as a betavoltaic battery: comparison of Si p-n and Ni/Si Schottky barrier. *Radiat Phys Chem*. 2016;125:205-212.

10. Wu M, Wang S, Ou Y, Wang W. Optimization design of betavoltaic battery based on titanium tritide and silicon using Monte Carlo code. *Appl Radiat Isot*. 2018;142:22-27.
11. Kim T, Lee N, Jung HK, Kim HJ. Enhancement of energy performance in betavoltaic cells by optimizing self-absorption of beta particles. *Int J Energy Res*. 2016;40(4):522-528.
12. Sun W, Kherani NP, Hirschman KD, Gadeken LL, Fauchet PM. A three-dimensional porous silicon p-n diode for betavoltaics and photovoltaics. *Adv Mater*. 2005;17(10):1230-1233.
13. Mohamadian M, Feghhi S, Afariadeh H. Geometrical optimization of GaN betavoltaic microbattery. In: *Proceedings of the 7th WSEAS International Conference on Power Systems*. China: Beijing:2007.
14. Duggirala R, Lal A, Radhakrishman S. *Radioisotope thin-film powered microsystems*. Ithaca, NY: Springer New York Dordrecht Heidelberg London; 2010.
15. Hui-yu X, Di Z. Development of high aspect ratio microstructures technology from abroad. *J Transducer Technol*. 2004.
16. Marty F, Rousseau L, Saadany B, et al. Advanced etching of silicon based on deep reactive ion etching for silicon high aspect ratio microstructures and three-dimensional micro- and nanostructures. *Microchem J*. 2005;36(7):673-677.
17. Di Cioccio L, Letertre F, Le Tiec Y, Papon AM, Jaussaud C, Bruel M. Silicon carbide on insulator formation by the Smart-Cut process. *Mater Sci Eng A*. 1997;B46:349-356.
18. Amarasinghe VP. Single crystalline silicon carbide thin film exfoliation for power device applications, New Brunswick, New Jersey: graduate program in department of chemistry and chemical biology, Rutgers, the State University of New Jersey, October 2015.
19. Russo J, Litz M, Ray W II, Rosen GM, Bigio DI, Fazio R. Development of tritiated nitroxide for nuclear battery. *Appl Radiat Isot*. 2017;125:66-73.
20. Russo J, Litz M, Ray W II, et al. Demonstration of a tritiated nitroxide nuclear battery. *Appl Radiat Isot*. 2018;144:93-103.
21. Demers H, Poirier-Demers N, Couture AR, et al. Three-dimensional electron microscopy simulation with the CASINO Monte Carlo software. *J Scanning Microscopes*. 2011;33(3):135-146.
22. Pelowitz D. "MCNPX User's Manual Version 2.7.0 LA-CP-11-00438," Los Alamos National Laboratory, 2011.
23. Lee S, Son S, Kim K, et al. Development of nuclear micro-battery with solid tritium source. *Appl Radiat Isot*. 2009;67(7–8):1234-1238.
24. Ellis BL, Fritzsche H, Patel J, Lang J, Suppiah S. Titanium tritide films as betavoltaic power sources. *Fusion Sci Technol*. 2017;71(4):660-665.
25. Kavetsky AG, Nekhoroshkov SN, Meleshkov SP, Kaminski YL, Akulov GP, Bower KE. Radioactive materials, ionizing radiation sources, and radioluminescent light sources for nuclear batteries. In: *polymers, phosphors, and voltaics for radioisotope microbatteries*. Boca Raton, FL: CRC; 2002:26-40.
26. Burks SR, Bakhshai J, Makowsky MA, et al. 2H,15 N-substituted nitroxides as sensitive probes for electron paramagnetic resonance imaging. *J Org Chem*. 2010;75(19):6463-6467.
27. Shanahan K, Holder J. Deuterium, tritium, and helium desorption from aged titanium tritides. *J Alloys Compd*. 2007;446–447:670-675.
28. Singh R, Cooper J, Melloch M, Chow T, Palmour J. SiC power Schottky and PiN diodes. *IEEE Trans Electron Devices*. 2002;49(4):665-672.
29. Liu L, Liu A, Bai S, Lv L, Jin P, Ouyang X. Radiation resistance of silicon carbide Schottky diode detectors in D-T fusion neutron detection. *Sci Rep*. 2017;7(1).
30. Chen X, Zhu H, Cai J, Wu Z. High-performance 4H-SiC-based ultraviolet p-i-n photodetector. *J Appl Phys*. 2007;102.
31. Klein C. Bandgap dependence and related features of radiation ionization energies in semiconductors. *J Appl Phys*. 1968;39(4):2029-2038.
32. Olsen LC. Review of betavoltaic energy conversion. In: *Washington State University and NASA, Richland*; 1992.
33. Hughes, H. G. I. and James M. R., "MCNP6," Los Alamos National Laboratory, 2014-02-27.
34. Russo J., Berk H. and Bigio D., "Effective coating of planar and HARMST surfaces for a tritiated nitroxide betavoltaic nuclear battery: the effects of crystallization rates," ARL-TR-8599, U.S. Army Research Laboratory, Adelphi, MD, Dec. 2018.
35. Myers-Ward RL, Hobart KD, Daniels KM, et al. Processing of cavities in SiC material for quantum technologies. *Mater Sci Forum*. 2018;924:905-907.
36. Liu B, Chen KP, Kherani NP, Zukotynski S. Power-scaling performance of a three-dimensional tritium betavoltaic diode. *Appl Phys Lett*. 2009;95(23):233112.

How to cite this article: Russo J, Litz MS, William Ray II, et al. Planar and textured surface optimization for a tritium-based betavoltaic nuclear battery. *Int J Energy Res*. 2019;1–20. https://doi.org/10.1002/er.4563